Cell, Vol. 118, 465–475, August 20, 2004, Copyright ©2004 by Cell Press

Cryo-EM Visualization of a Viral Internal Ribosome Entry Site Bound to Human Ribosomes: The IRES Functions as an RNA-Based Translation Factor

Christian M.T. Spahn,[1,2,4,7] Eric Jan,[5,7] Anke Mulder,[1,2,6] Robert A. Grassucci,[1,2] Peter Sarnow,[5] and Joachim Frank[1,2,3,*]
[1]Howard Hughes Medical Institute
Health Research Inc. at
[2]Wadsworth Center
Empire State Plaza
Albany, New York 12201
[3]Department of Biomedical Science
The State University of New York at Albany
Albany, New York 10012
[4]Institut für Medizinische Physik und Biophysik
Charité-Universitätsmedizin Berlin
Ziegelstrasse 5–9
10117 Berlin
Germany
[5]Department of Microbiology and Immunology
Stanford University School of Medicine
Stanford, California 94305
[6]Department of Biology
Purdue University
West Lafayette, Indiana 47906

Summary

Internal initiation of protein synthesis in eukaryotes is accomplished by recruitment of ribosomes to structured internal ribosome entry sites (IRESs), which are located in certain viral and cellular messenger RNAs. An IRES element in cricket paralysis virus (CrPV) can directly assemble 80S ribosomes in the absence of canonical initiation factors and initiator tRNA. Here we present cryo-EM structures of the CrPV IRES bound to the human ribosomal 40S subunit and to the 80S ribosome. The CrPV IRES adopts a defined, elongate structure within the ribosomal intersubunit space and forms specific contacts with components of the ribosomal A, P, and E sites. Conformational changes in the ribosome as well as within the IRES itself show that CrPV IRES actively manipulates the ribosome. CrPV-like IRES elements seem to act as RNA-based translation factors.

Introduction

Accurate selection of the start site in an mRNA by the translational machinery requires binding of the mRNA to the small 40S subunit, positioning of the initiator tRNA at the start codon, and joining of the 60S subunit to form an elongation-competent ribosome. Canonical eukaryotic cap-dependent translation initiation follows a complex pathway that is facilitated by a large number of protein initiation factors, which interact with the ribosome, the mRNA, the initiator tRNA, and one another (Dever, 2002; Sonenberg and Dever, 2003). An alternative pathway of translation initiation exists that involves structured RNA sequences, called internal ribosome entry sites (IRESs), which allow initiation in a 5′ end-independent manner (Hellen and Sarnow, 2001; Vagner et al., 2001). IRES elements have been discovered in several viral and cellular RNA elements and are preferentially used to hijack the translational apparatus of the host during viral infection and to initiate translation of specific mRNAs during cellular stress or other periods when overall global translation is compromised (Hellen and Sarnow, 2001; Sachs, 2000; Vagner et al., 2001).

Various types of IRESs exist that initiate translation via distinct mechanisms requiring specific canonical initiation factors (Hellen and Sarnow, 2001; Vagner et al., 2001). For example, the poliovirus IRES requires all of the canonical initiation factors except for the cap binding protein eIF4E to recruit the ribosomal 43S preinitiation complexes (Pestova et al., 1996). Other IRESs, such as the hepatitis C virus (HCV) IRES, require only eIF3, eIF2, and initiator Met-tRNA to assemble 80S ribosomes (Pestova et al., 1998). In contrast, a novel class of IRESs has recently been found in the cricket paralysis virus-like viruses (CrPV) that can directly assemble elongation-competent ribosomes in the absence of canonical initiation factors and initiator Met-tRNA (Pestova and Hellen, 2003; Sasaki and Nakashima, 1999, 2000; Wilson et al., 2000b). Biochemical studies have suggested that the IRES occupies the ribosomal P site and sets the translation frame such that the first codon is positioned in the A site. The IRES undergoes an unusual first translocation step without peptide bond formation. This translocation event requires eEF1A, which delivers the first aminoacylated tRNA to the A site, and eEF2, which catalyzes the translocation of the aminoacylated tRNA from the A site to the P site (Jan et al., 2003; Pestova and Hellen, 2003). At this stage, the resulting ribosomal complex with an aminoacylated tRNA in the P site resembles a canonical 80S initiation complex and can proceed in a normal elongation cycle. Therefore, it appears that the CrPV IRES jumpstarts translation in the elongation phase (Jan et al., 2003; Pestova and Hellen, 2003; Wilson et al., 2000a).

To investigate the molecular mechanism by which the CrPV IRES recruits the ribosome, we have generated 3D reconstructions of the CrPV IRES bound to human ribosomal particles using single-particle cryo-EM. We show that a defined structure of the CrPV IRES is located in the ribosomal intersubunit space and forms specific contacts with both the 40S and the 60S subunit. Moreover, CrPV IRES binding at components of the ribosomal A, P, and E sites actively manipulates the ribosome by inducing conformational changes. In addition, conformational changes also occur in the IRES itself. Since such features have been previously observed with protein translation factors, we propose that CrPV-like IRES elements are RNA-based translation factors.

*Correspondence: joachim@wadsworth.org
[7]These authors contributed equally to this work.

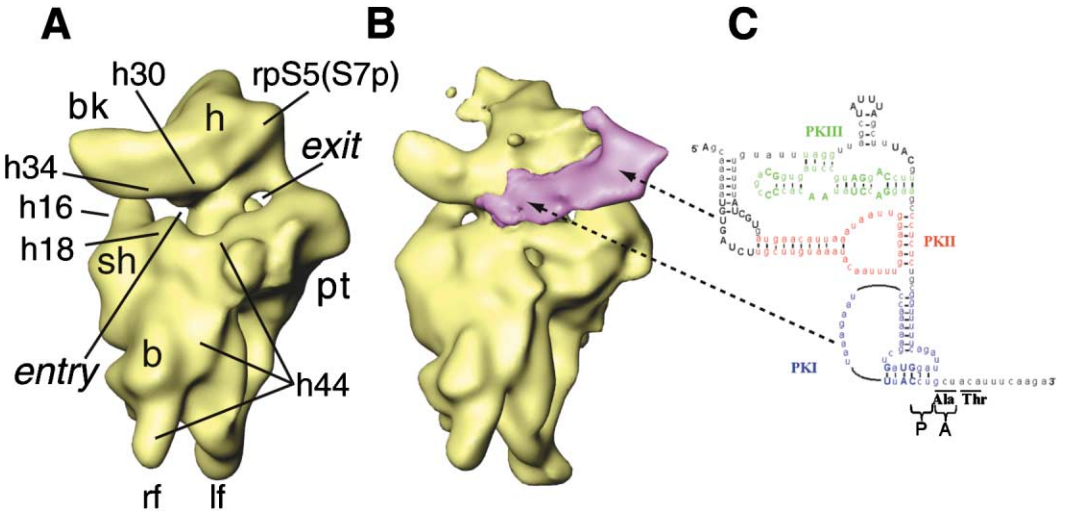

Figure 1. Cryo-EM Maps of the Vacant 40S Subunit and the 40S•CrPV IRES Complex

Surface representations of the human ribosomal 40S subunit derived from HeLa cells (A) and the 40S subunit in complex with the CrPV IRES (B). The 40S subunit is painted yellow; density corresponding to the IRES is pink. The subunits are shown from the intersubunit side. Landmarks for the 40S subunit are the following: b, body; bk, beak; h, head; lf, left foot; rf, right foot; pt, platform; and sh, shoulder. The entry and exit channels for the mRNA (Frank et al., 1995, 2000; Yusupova et al., 2001) are designated "entry" and "exit." The position of five 18S rRNA helices (h16, h18, h30, h34, and h44) and of protein rpS5 are indicated, as identified by comparison with a cryo-EM map of the yeast 80S ribosome (Spahn et al. [2001a], also see Figure 4). (C) Secondary structure diagram of the CrPV IRES (Jan and Sarnow, 2002; Kanamori and Nakashima, 2001). Nucleotides belonging to pseudoknots PK I–PK III and to stem loop 1 (SL1) are painted in different colors. Conserved nucleotides within the CrPV-like virus family are represented by capital letters. The triplets that are positioned in the P and A sites during the first A site occupation are designated P and A, respectively. Ala and Thr refer to the first two amino acids that are incorporated into the viral protein. The dashed arrows indicate the tentative location of PKI and PKII/III in the cryo-EM density map.

Results and Discussion

Cryo-EM Reconstructions of Human Ribosomal Particles in Complex with the CrPV IRES

Using purified human 40S and 60S ribosomal subunits from HeLa cells, we obtained maps of the CrPV IRES in complex with 40S subunits and with 80S ribosomes, which had been reassociated in the presence of the IRES, at resolutions of 20.3 Å and 17.3 Å, respectively (Figures 1 and 2, and see Supplemental Table S1 at http://www.cell.com/cgi/content/full/118/4/465/DC1). A comparison of these maps with control maps of the vacant 40S subunit and the vacant reassociated 80S ribosome shows that density attributable to the CrPV IRES is directly visible in both the 40S and 80S complexes (Figures 1 and 2). The additional nonribosomal densities appear to be large enough to accommodate the IRES in its entirety. Accordingly, a defined tertiary fold of the CrPV IRES forms specific intermolecular contacts with the ribosomal particles, likely for the purpose of hijacking the ribosome.

Architecture of the Human 80S Ribosome

In order to facilitate analysis of the intermolecular contacts on the molecular level, we compared the structure of the human 80S ribosome with previous cryo-EM structures of the *E. coli* 70S ribosome and the yeast 80S ribosome (Figure 3). In particular, we make reference to a molecular model for the evolutionarily conserved core of the eukaryotic 80S ribosome based on the cryo-EM structure of the yeast 80S ribosome (Spahn et al., 2001a) (Figure 4). For the comparison, we used the cryo-EM map of the 80S•CrPV IRES complex, since it had a better resolution than the map of the vacant 80S ribosome. In agreement with previous analysis of other mammalian ribosomes (Dube et al., 1998; Morgan et al., 2000, 2002), the core of the human 80S ribosome shows strong overall similarity with the core of the yeast 80S ribosome and the *E. coli* 70S ribosome while containing additional mass in the periphery (Figure 3).

Differences that exist in the core of the yeast 80S ribosome compared to the bacterial 70S ribosome, e.g., the changed position of helix 16 of the small subunit (SSU) rRNA or the truncation of helix 17 of the SSU rRNA, are also present in the human 80S ribosome (Figures 3D–3F). Bringing the cryo-EM map of the human 80S ribosome into the same orientation as the map of the yeast 80S ribosome by computationally aligning the 60S subunit portions of the two maps resulted in a good overall fit of the atomic model of the core of the yeast 80S ribosome with the core of the cryo-EM map of the human 80S ribosome (Figure 4). The good fit extended to most parts of the 40S subunit, i.e., body and platform domains, showing that the ratchet-like subunit rearrangement (see Spahn et al. [2004]) is not present in the human 80S•CrPV IRES complex, which is largely in the same conformation as the posttranslocational yeast 80S ribosome. The only required change in the atomic model was a rotation of the components of the 40S subunit head due to a conformational change caused by the CrPV IRES (see below).

Most of the additional density of the human 80S ribosome, compared to the yeast 80S ribosome, is due to the size increase of expansion segments in the rRNAs,

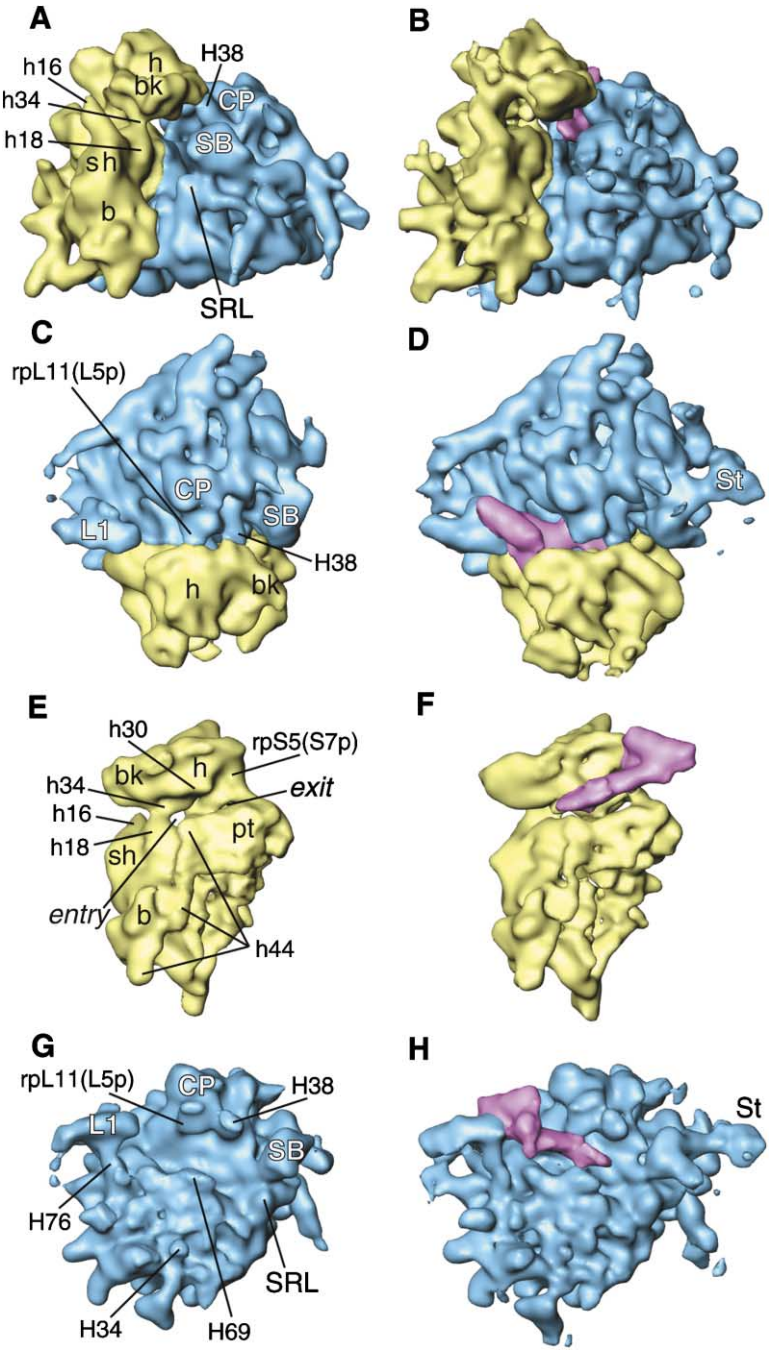

Figure 2. Cryo-EM Maps of the Vacant Human 80S Ribosome and of the 80S•CrPV IRES Complex

(A, C, E, and G) Vacant, reassociated 80S ribosome isolated from HeLa cells. (B, D, F, and H) 80S•CrPV IRES complex. (A) and (B), side view; (C) and (D), top view; (E) and (F), view from the 60S side, with 60S removed; and (G) and (H), view from the 40S side, with 40S removed. The ribosomal 40S subunit is painted yellow, the 60S subunit blue, and the CrPV IRES pink. Landmarks for the 60S subunit are the following: CP, central protuberance; L1, L1 protuberance; SB, stalk base; and SRL, sarcin-ricin loop. Several helices of the 28S rRNA are designated, as well as protein rpL11. The positions of these components were obtained by docking the molecular model for the yeast 80S ribosome (Spahn et al., 2001a) into the cryo-EM map of the human 80S ribosome (see Figure 4). "St" in (D) and (H) designates the extended stalk that becomes visible in the 80S•CrPV IRES complex. Labels for the 40S portion are as in Figure 1.

with the human 18S rRNA (1869 nucleotides) being 71 nucleotides larger than the yeast 18S rRNA (1798 nucleotides) and the human 28S rRNA (5025 nucleotides) being 1629 nucleotides larger than the yeast 25S rRNA (3396 nucleotides). The biggest contribution to the increased size of the 18S rRNA is made by expansion segment ES3 (Gerbi, 1996), which is 45 nucleotides longer in the human 18S rRNA. Accordingly, the left foot of the human 40S subunit is enlarged (Figures 3A and 3D), in line with our previous identification of ES3 in the yeast 40S subunit, and a tertiary interaction takes place between ES3 and ES6 (Alkemar and Nygard, 2004; Spahn et al., 2001a).

The extra density in the human 60S ribosomal subunit can be largely attributed to the increase in size and complexity of the expansion segments in the 28S rRNA. The position of the extra density is in good agreement with our previous identification of expansion segments in yeast (Spahn et al., 2001a), allowing the tentative identification of the additional parts of the human expansion segments (Figures 3G, 3J, and 3M). The largest increase is present in ES7, which is increased by 655 nucleotides in the human 28S rRNA compared to the yeast 25S rRNA. A smaller part of this extra density can be observed below the stalk base, whereas the larger portion forms the V-shaped feature at the back of the

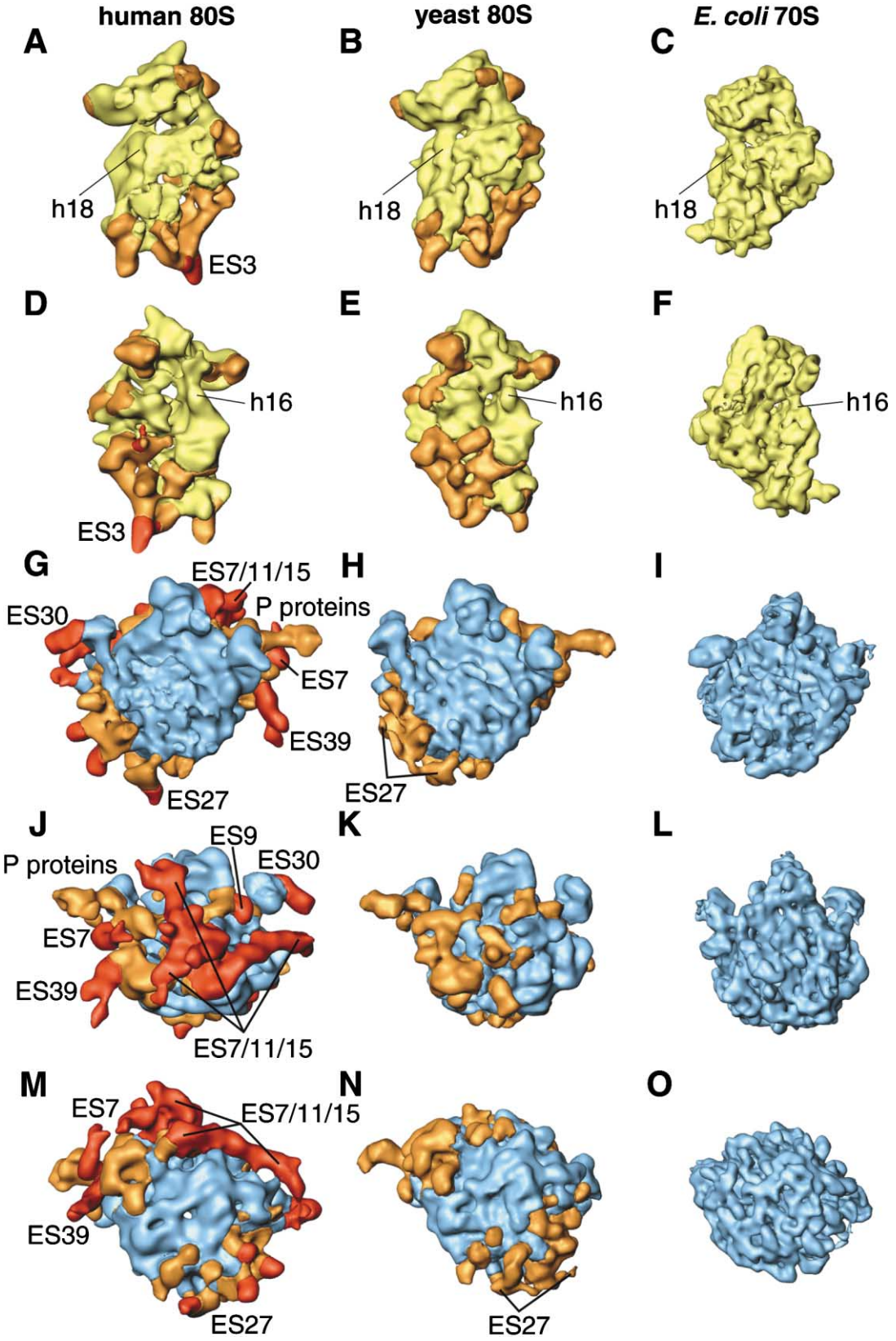

Figure 3. Comparison of the Architecture of Ribosomes from Human, Yeast, and *E. coli*

Computationally isolated ribosomal subunits of the cryo-EM maps of the human 80S•CrPV IRES complex (A, D, G, J, and M), the translating yeast 80S ribosome (B, E, H, K, N) (Spahn et al., 2001a), and the *E. coli* 70S ribosome (C, F, I, L, O) (Gabashvili et al., 2000). The evolutionarily conserved cores of the small 30S and 40S subunits are painted yellow, the cores of the large 50S and 60S subunits blue. Extra density present in both cytoplasmatic eukaryotic 80S ribosomes is painted orange, whereas density present only in 80S ribosomes from human is painted red. The small ribosomal subunits are shown from the inter-subunit face (A–C) and from the solvent side (D–F). The large ribosomal subunits are shown from the intersubunit face (G–I), the back side (J–L), and from the membrane attachment side facing the exit tunnel (M–O). The position of some expansion segments in 18S or 25/28S rRNA is indicated.

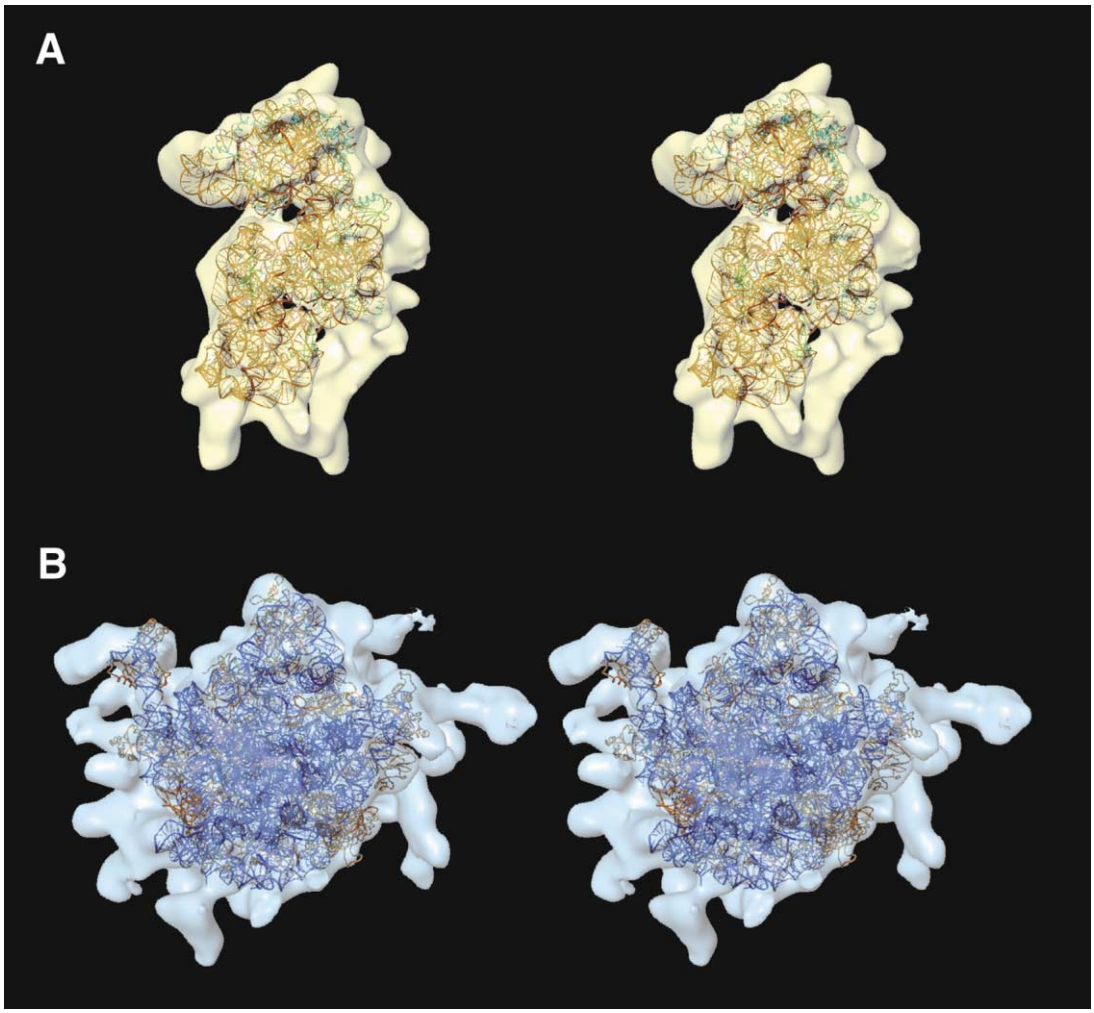

Figure 4. Docking of Molecular Models into the Evolutionarily Conserved Core of the Human 80S Ribosome

Stereoviews of the docking of atomic models for the evolutionarily conserved core of the yeast 80S ribosome (Spahn et al., 2001a) into the cryo-EM map of the human 80S•CrPV IRES complex are shown for the 40S subunit (A) and the 60S subunit (B). Density maps for the corresponding ribosomal subunits were computationally isolated and are shown as semitransparent contours from their intersubunit faces. The atomic models are shown in ribbon representation. 18S rRNA is in yellow, small ribosomal subunit proteins in cyan, 5S/5.8S/28S rRNA in blue, and large ribosomal subunit proteins in orange.

solvent side of the 60S subunit (Morgan et al., 2002) together with enlargements of ES11 and ES15. ES30 is an extension of helix 78 of 28S rRNA and accordingly constitutes additional density present at the top of the L1 protuberance (Figures 3G and 3J) similar to the canine 80S ribosome (Morgan et al., 2002). Moreover, additional density is present to explain the larger expansion segments ES9 and ES39. Surprisingly, there is no density to account for the huge increase in size of ES27, which is 547 nucleotides larger in human 28S rRNA than in yeast 25S rRNA. Even the part of this expansion that is present in the 80S ribosome from yeast (Spahn et al., 2001a) is largely missing in the reconstruction of the human 80S ribosome (compare Figures 3G and 3H). A likely explanation is that ES27 does not occur in consistent positions in the molecule population, in view of our previous finding in yeast that ES27 is flexible and assumes different orientations, differing by as much as 90 degrees (Beckmann et al., 2001).

The architecture of the human 80S ribosome is very similar to the architecture of the yeast 80S ribosome but with enlarged expansion segments at the periphery. The yeast 80S ribosome in turn contains a core that largely resembles the prokaryotic ribosome (Spahn et al., 2001a). Like the common parts of the expansion segments, which are present in both the yeast and the human 80S ribosomes, the structural components visible as additional mass in the human ribosome appear to engage in additional tertiary and quaternary interactions. In summary, the human 80S ribosome is built from (1) an evolutionarily conserved core, (2) additional components that are present in yeast 80S ribosomes as well, and (3) components that appears to be specific for ribosomes from higher eukaryotes (Figure 3).

Binding of the CrPV IRES to the Ribosomal 40S Subunit

In the binary complex of the 40S subunit with the CrPV IRES, the IRES interacts with the head of the 40S subunit on the intersubunit side (Figure 1B). Overall, the IRES

has an elongate shape. A relatively globular part interacts with the head of the 40S subunit in the region of protein rpS5(S7p) (Spahn et al., 2001a), overlapping with the binding region for the E site tRNA (Figure 6G). From there, the IRES traverses the P site near helix 30 of the 18S rRNA (Spahn et al., 2001a) and extends into the decoding center at the A site, formed by helices 18 and 34 of the 18S rRNA and the top of helix 44. To some extent, extra density also appears to occupy the mRNA entry channel. At this resolution, it is not possibly to tell if the occlusion of the mRNA entry channel is due to a conformational change or due to IRES RNA density. However, it might well be that the single-stranded 3′ part of the IRES RNA is already threaded into the mRNA entry channel and contributes to filling the channel.

The secondary structure of the CrPV IRES (Figure 1C) contains three prominent pseudoknots, termed PK1, PK2, and PK3 (Jan and Sarnow, 2002; Kanamori and Nakashima, 2001). Previous biochemical studies determined that PK1 occupies the ribosomal P site in the 40S•CrPV IRES complex and is situated adjacent to the first encoded codon (GCU for Ala). Therefore, PK1 most likely forms the extended part of the IRES, whereas PK2 and PK3 form the more globular partition that is located in the E site region (Figure 1). Binding of the CrPV IRES to the 40S subunit occurs in regions that are also involved in tRNA binding to the A, P, and E sites and that are therefore functionally important and evolutionarily well conserved. This behavior is strikingly different from the binding of HCV IRES, which has been shown to interact mainly at the evolutionarily more divergent solvent side of the 40S subunit at the back of the platform (Spahn et al., 2001c). However, there is some overlap in binding sites in the E site region for these two IRES elements.

Binding of the CrPV IRES to the 80S Ribosome

After formation of the 80S•CrPV IRES complex by the association of the ribosomal 60S subunit with the IRES bound 40S subunit, the IRES perches in the intersubunit space, in a position similar overall to its position in the 40S•IRES complex (compare Figures 1B and 2F), where it interacts with specific components of the 40S and the 60S subunit (Figure 5). However, the IRES has apparently retracted itself to some extent from the A site region and moved toward the E site region (see Figure 6, in particular 6G versus 6H). This movement appears to be facilitated by a conformational change of the IRES, leading to a more pronounced globular shape of the IRES density and a thinner elongate portion. The movement of the IRES upon subunit association alters its interaction with the 40S subunit in the 80S•IRES complex as compared to its interaction in the 40S•IRES complex. Although in the 80S•IRES complex intermolecular contacts are still formed with the helix 30 region and the rpS5 (S7p) region of the 40S subunit, there is no interaction of the IRES with the 40S subunit between these two regions, while the interaction of the IRES with the rpS5 region appears to be intensified (Figures 5 and 6).

The movement and conformational change of the CrPV IRES upon subunit association is probably induced by its interaction with the 60S subunit. Three contact regions can be observed on the 60S subunit (Figures 2D, 2H, and 5): (1) the L1 protuberance, which is built by rpL1 (L1p) and helices 76–78 of the 28S rRNA; (2) the central protuberance at the position of rpL11 (L5p); and (3) helix 69 of 28S rRNA, which participates in the formation of the intersubunit bridge B2a (Spahn et al., 2001a; Yusupov et al., 2001). The L1 protuberance contacts the globular part of the CrPV IRES, while rpL11 (L5p) and helix 69 of 28S rRNA interact with the extended part of the IRES. Interestingly, these ribosomal components are part of the universally conserved tRNA binding sites, similar to the 40S subunit components that form tentative contacts with the CrPV IRES (Figures 5 and 6). Protein rpL11 (L5p) and helix 69 of 28S rRNA interact with the P site tRNA at the T and D loops, respectively, whereas the L1 protuberance interacts with the T loop of the E site tRNA (Agrawal et al., 2000; Morgan et al., 2002; Spahn et al., 2001a; Yusupov et al., 2001). Binding to evolutionarily conserved regions of both ribosomal subunits may explain why the CrPV IRES is active not only in higher eukaryotes but also in yeast (Thompson et al., 2001).

Conformational Changes in the Ribosome upon CrPV IRES Binding

The ribosome responds to the binding of the CrPV IRES with a conformational change (Figure 7). Thus, the CrPV IRES actively manipulates the translational machinery, as was previously established for the HCV IRES (Spahn et al., 2001c). Although the binding sites of the two IRESs are quite different, the conformational changes that they induce in the 40S ribosomal subunit bear remarkable similarities. The head of the 40S subunit rotates relative to the body in the 40S•CrPV IRES complex, which results in a different beak position. This movement is accompanied by more localized changes; for example, an additional connection emerges at the solvent side of the head and the shoulder (Figure 7B). This connection appears to be brought about by a movement of ribosomal proteins located in the beak, among them rpS3 and helix 16 of the 18S rRNA at the shoulder (Figure 4).

Helix 16 is a very interesting ribosomal component. Although its presence is evolutionarily conserved, its position is different in bacteria and eukaryotes (Spahn et al., 2001a). In eukaryotes, it projects into the solvent (Figures 3D and 3E), being rotated about 90° relative to the position of helix 16 in prokaryotes, where it is folded toward helix 18 of the 16S rRNA, the so-called 530 pseudoknot structure (compare Figures 3D and 3E versus 3F). Helix 18, in turn, is involved in forming the noncovalent latch structure with helix 34 of the head domain. The latch is part of the mRNA entry channel, as it clamps the incoming 3′ strand of the mRNA (Frank et al., 1995, 2000; Lata et al., 1996; Schlünzen et al., 2000; Wimberly et al., 2000; Yusupova et al., 2001). Protein rpS3 is part of the mRNA entry channel as well.

The finding that two unrelated IRESs provoke similar conformational changes at the mRNA entry channel (compare Figures 7A and 7E with 7B and 7F, respectively) suggests that these changes are part of a general mechanism for translation initiation. The similarity of the changes in the two systems corroborates our previous suggestion that such conformational manipulations in

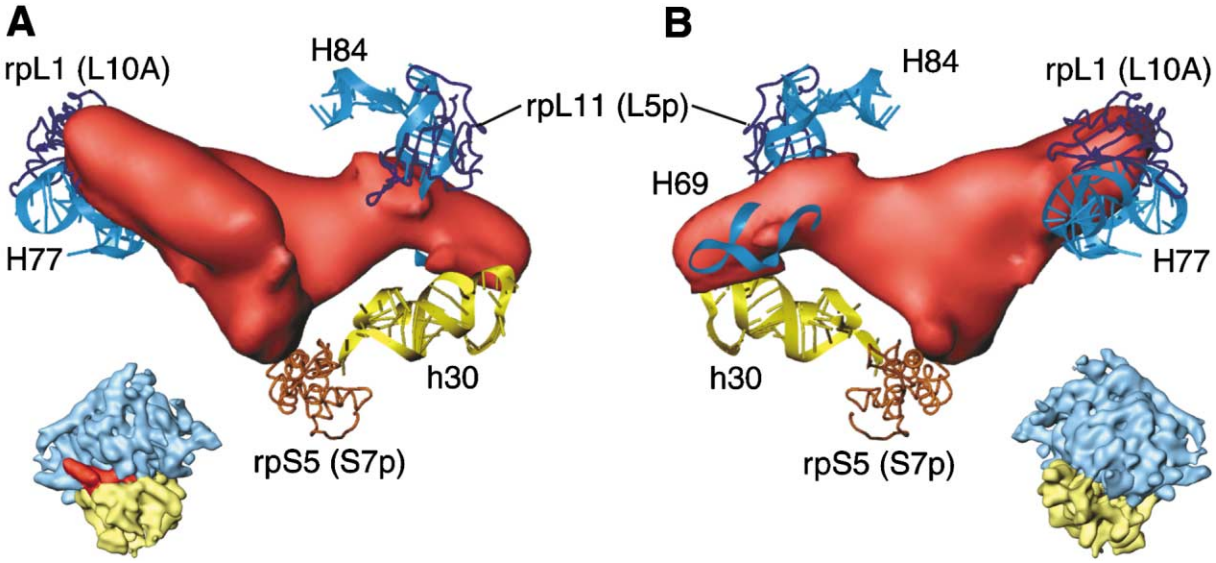

Figure 5. Interaction of the CrPV IRES with Ribosomal Components

Cryo-EM density corresponding to the CrPV IRES in the 80S•CrPV IRES complex is shown in red, together with atomic models of ribosomal components that are located at the observed interaction sites. The atomic models were derived by docking the model of the evolutionarily conserved core of the yeast 80S ribosome (Spahn et al., 2001a) into the cryo-EM map of the complex (Figure 4). The views are from the top of the 80S ribosome (A) and from the membrane attachment side (top view rotated by about 180°). Thumbnails are included as an orientation aid.

the HCV IRES case are related to the threading of the 3′ part of the mRNA into the mRNA entry channel (Spahn et al., 2001c). The finding also reinforces the view that the altered position of helix 16 is related to differences in the mechanism of translation initiation in prokaryotes and eukaryotes (Doudna and Rath, 2002; Spahn et al., 2001a). The positioning of helix 16 of 18S rRNA away from the latch of the mRNA entry channel in eukaryotes might result in greater flexibility, thereby facilitating dynamic changes of the latch. Moreover, the changed position of helix 16 at the shoulder allows the observed interaction with rpS3 at the head, which in turn might also facilitate the opening of the mRNA entry channel.

Upon the joining of the 60S subunit to the 40S•CrPV IRES complex, the rotational movement of the head of the 40S subunit is reversed, i.e., the head overall has the same relative position in the 80S•CrPV IRES complex as in the 80S control (Figure 2). However, the interaction between helix 16 of the 18S rRNA and ribosomal proteins from the head seen in the 40S•CrPV IRES complex persists in the 80S•CrPV IRES complex but is not seen in the 80S control, suggesting that it is the binding of the CrPV IRES that results in this interaction (Figures 7C and 7D). In contrast, the strong latch interaction between helices 18 and 34 of the 18S rRNA, although present in the vacant 80S ribosome, appears to be more open in the 80S•CrPV IRES complex (Figures 2E and 2F), possibly making the ribosomal A site more accessible for delivery of the aminoacylated tRNA. Compared to the 40S•CrPV IRES complex, where the mRNA channel appears to be narrow or even closed, subunit association leads to an opening up of the entry channel in the 80S•CrPV IRES complex (Figure 7B versus Figure 7D). This conformational change might provide more flexibility for the coding part of the viral RNA, which in turn might also be necessary for ternary complex binding and decoding of the first codon.

On the 60S subunit side, the presence of the CrPV IRES during subunit association leads to a conformational change in the stalk region. The ribosomal P proteins are disordered in the vacant 80S ribosome but become ordered due to the presence of the CrPV IRES, yielding strong density for the stalk in the 80S•CrPV IRES complex (Figures 2C, 2D, 2G, 2H, 7C, and 7D). The induction of the extended stalk by ribosomal ligands has been previously observed, notably by EF-G in prokaryotes (Agrawal et al., 1999) and by eEF2 in yeast (Agrawal et al., 1999; Gomez-Lorenzo et al., 2000). Since the ribosomal P proteins are implicated in interaction and GTPase activation of translation factors, the CrPV IRES may act to induce the conformational change in the stalk region, a change required to facilitate the next steps of the pathway of translation initiation, i.e., ternary complex binding and eEF2-dependent translocation.

Mechanism of CrPV IRES-Induced Internal Initiation of Translation

Taken together, the cryo-EM structures presented here are not only in excellent agreement with findings of previous biochemical studies (Jan et al., 2003; Jan and Sarnow, 2002; Nishiyama et al., 2003; Pestova and Hellen, 2003; Wilson et al., 2000a), they also shed light on the molecular mechanism of the CrPV IRES and on its unusual mode of initiating translation. (1) The CrPV adopts a tertiary fold that gives it a high affinity for the 40S subunit due to specific intermolecular interactions. The interaction of the PK2 and PK3 portions of the IRES with the E site region (Figure 1) could provide the net binding energy, since deletion or disruption of PK1 barely affects ribosomal binding of the IRES (Jan and Sarnow, 2002; Nishiyama et al., 2003). (2) PK1 interacts with the P site region of the ribosome (Figure 1), and this interaction appears to be crucial for the correct

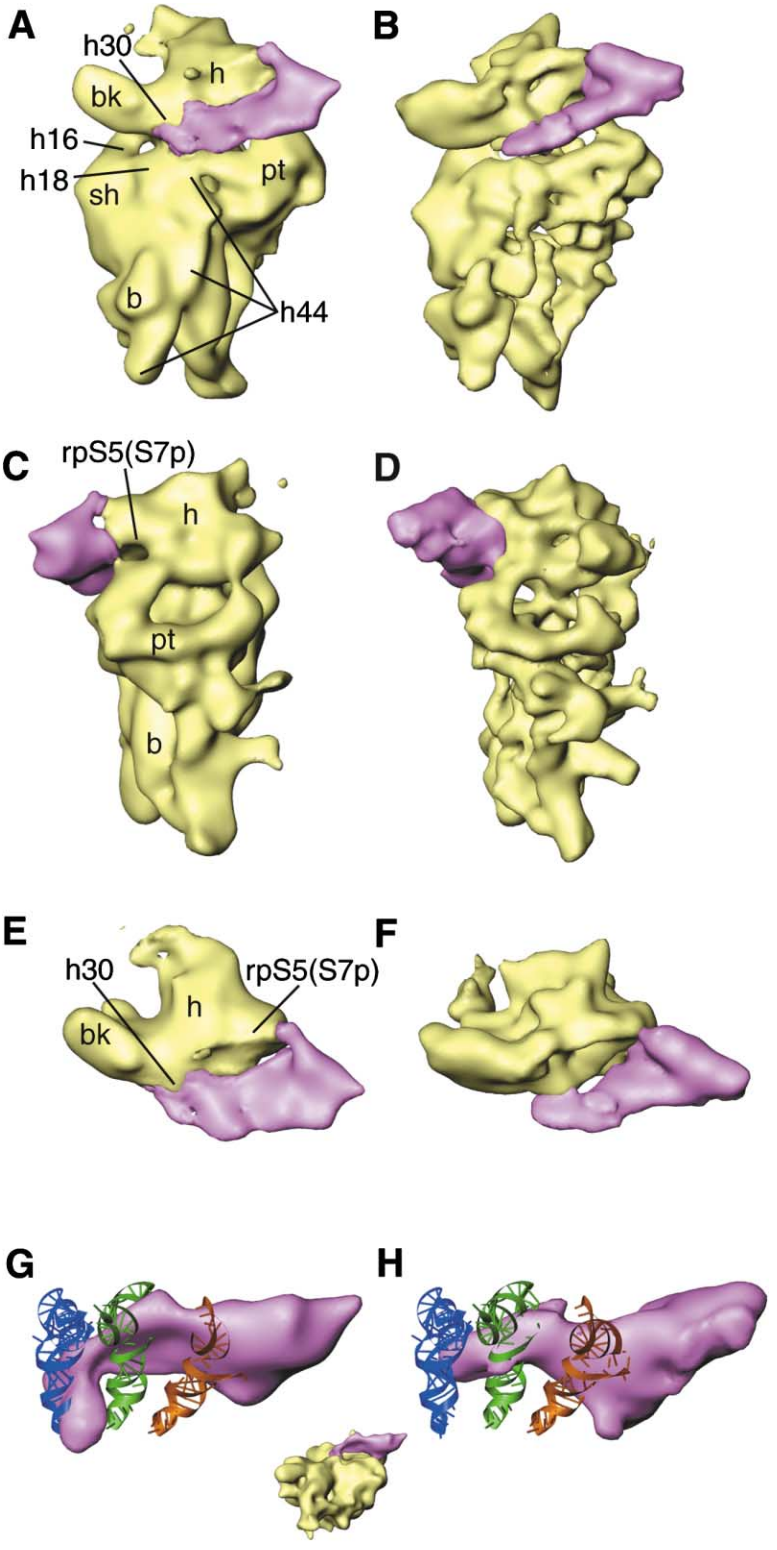

Figure 6. The CrPV IRES Interaction with the 40S Subunit Compared to its Interaction with the 40S Portion of the 80S Ribosome

40S•CrPV IRES complex (A, C, E, and F) and 80S•CrPV IRES complex with the 60S subunit computationally removed (B, D, F, and H). The 40S subunit is painted yellow, and the density corresponding to the IRES is pink. (A and B) View from 60S side; (C and D) view from the platform side. In (E) and (F), density from only the head domain of the 40S subunit is shown in a top view, together with the IRES density. (G) and (H) show the IRES density superposed onto atomic models in ribbon representation that indicate the putative binding positions. The A site tRNA is painted blue, the P site tRNA green, and the E site tRNA orange. The tRNA coordinates (Yusupov et al., 2001) were superposed onto the P site tRNA of the yeast 80S ribosome (Spahn et al., 2001a), which had the same orientation as the CrPV IRES complexes. The view is from the bottom of the 40S subunit along the long axis of the subunit, as indicated by the thumbnail. Labels are as in Figure 1.

positioning of the first codon in the decoding center (Jan and Sarnow, 2002; Nishiyama et al., 2003). (3) Moreover, the binding of the CrPV IRES leads to a pronounced conformational change in the 40S subunit, particularly in the latch region (Figures 1, 2, and 7). This conformational rearrangement could facilitate threading of the coding part of the viral RNA into the mRNA entry channel. (4) The CrPV IRES also forms specific contacts with the 60S subunit (Figure 5), which could aid and guide the process of subunit association. (5) Moreover, the CrPV IRES produces a conformational change in the stalk region, which is part of the factor binding site of the

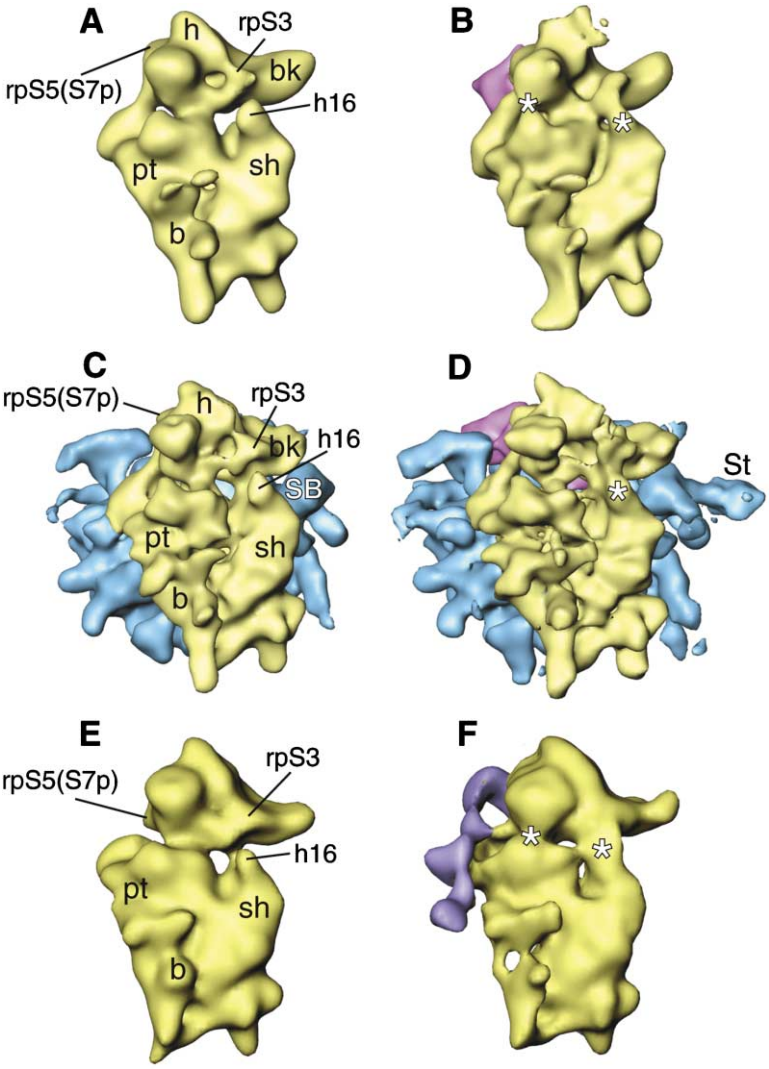

Figure 7. IRES-Induced Conformational Changes in Mammalian Ribosomes

Human 40S subunit (A), human 40S•CrPV IRES complex (B), human 80S ribosome (C), human 80S•CrPV IRES complex (D), rabbit 40S subunit (E), and rabbit 40S•HCV IRES complex (F). All reconstructions are viewed from the 40S subunit solvent side with the 40S subunit painted yellow, the 60S subunit blue, the CrPV IRES pink, and the HCV IRES purple. The maps of the rabbit 40S subunit (E) and the corresponding 40S•HCV IRES complex (F) are taken from (Spahn et al., 2001c). Labels are as in Figures 1 and 2. Some conformational changes in the various IRES complexes (B, D, and F) are indicated with asterisks, and the CrPV IRES-induced extended stalk (D) is labeled "St." For further details, see text.

ribosome (Figure 2). This change may prime the 80S ribosome for the subsequent events that require interaction with elongation factors eEF1A and eEF2. (6) Finally, interaction with the 60S subunit leads to a conformational change in the CrPV IRES itself and its movement relative to the 40S subunit, rendering the A site more accessible (Figure 6). These conformational changes might be related to the observed flexibility of the IRES (Jan and Sarnow, 2002) and its ability to undergo a translocation reaction, since the IRES has to free up the P site region during the first translocation step.

In this context, it is also of interest that the CrPV IRES interacts with the ribosome in the same regions as do the tRNAs (Morgan et al., 2002; Spahn et al., 2001a; Yusupov et al., 2001), the physiological substrate for the translocation reaction. A divergent RNA element might mimic part of the tRNAs in order to bind to and manipulate the ribosome. Therefore, the IRES most likely makes use of the intrinsic mechanism of ribosomal translocation. An understanding of the specific RNA elements in the CrPV IRES that interact with the ribosome may shed light on the normal interactions of E and P site tRNAs with the ribosome.

One of the surprising results from the cryo-EM structure of the 40S•HCV IRES complex was that a viral IRES RNA can actively manipulate the translational apparatus (Spahn et al., 2001c). The same principle is now seen to hold for the CrPV IRES. Although unrelated in sequence, structure, and mechanism, the two IRESs induce similar conformational changes in the ribosome (Figure 7). A probable explanation is that these conformational changes are an integral part of the general mechanism of translation initiation and are required, for example, to thread the mRNA into the ribosomal entry and exit channels for the mRNA (Frank et al., 1995; Yusupova et al., 2001). In particular, defined movements of the head domain of the 30S or 40S ribosomal subunit appear to be crucial for this mechanism (Carter et al., 2001; Lata et al., 1996; Spahn et al., 2001c) and also for the mechanism of translation elongation (Gao et al., 2003; Spahn et al., 2004; Valle et al., 2003).

Since translation factors are known to function via the induction of specific conformational changes in the ribosome (Carter et al., 2001; Frank and Agrawal, 2000; Gomez-Lorenzo et al., 2000; Ogle et al., 2002; Spahn et al., 2004; Stark et al., 2000), similar conformational

changes may therefore occur in the steps of canonical translation initiation as well. Thus, the CrPV IRES acts in principle like a translation factor by inducing ribosomal conformations that are required for a particular step of translation to occur. In this sense, this IRES not only replaces protein translation factors but in fact also functions as an RNA-based translation factor that is covalently attached to the mRNA.

Experimental Procedures

Isolation of Ribosomal Subunit and CrPV IRES and Complex Formation

40S and 60S ribosomal subunits were purified as described from HeLa S3 spinner cells (National Center for Research Resources) (Jan and Sarnow, 2002). Western blot analysis verified the absence of eIF2 contamination. The purity and integrity of 40S and 60S subunits was also examined by detection of 18S and 28S rRNAs by ethidium staining. The concentration of 40S and 60S subunits was determined by spectrophotometry using the conversions 1 A260 = 50 pmol for 40S and 1 A260 = 25 pmol for 60S subunits (Matasova et al., 1991). The assembly activities of 40S and 60S subunits to wild-type IRES elements were determined by sucrose gradients and gel shift assays (Jan and Sarnow, 2002).

Vacant 40S subunits, vacant 80S ribosomes, and 40S•IRES and 80S•IRES complexes were assembled in Buffer E (20 mM Tris [pH 7.5], 100 mM potassium acetate, 2.5 mM magnesium acetate, 0.25 mM spermidine, 2 mM DTT). 40S subunits (200 nM), 200 nM of 60S subunits, and a 10-fold molar excess of CrPV IRES RNAs were used. Assembly of 40S and 80S complexes was determined by sucrose gradient analysis (>95% assembled). CrPV IRES RNA was synthesized in vitro as described (Jan and Sarnow, 2002).

Cryo-EM and 3D Reconstruction

Samples of 40S subunits (final concentration [f.c.] approximately 50 nM) or 80S ribosomes (f.c. approximately 30 nM) were applied to cryo-EM grids and shock frozen in liquid ethane (Dubochet et al., 1988; Wagenknecht et al., 1988). Micrographs were recorded under low-dose conditions on a Philips F20 (FEI/Philips, Eindhoven) at a magnification of about 52,000 for the 40S•CrPV IRES complex. Micrographs for the vacant 40S subunit, the vacant 80S ribosome, and the 80S•CrPV IRES complex were taken on a Philips F30 (FEI/Philips, Eindhoven) at a magnification of about 38,000 (see Table S1 on the *Cell* web site). The micrographs were scanned on a Zeiss flatbed scanner (Z/I Imaging Corporation, Huntsville, AL) with a step size of 14 μm, resulting in a pixel size of 3.66 Å on the object scale for data recorded on the F30 microscope. The pixel size for the F20-derived 40S•CrPV IRES complex was originally 2.82 Å on the object scale and was later adjusted by interpolation to match that of the other specimen. The data were analyzed using the SPIDER system (Frank et al., 1996). After automated particle selection and visual verification, the data sets were subdivided into defocus groups (Table S1). Refined CTF-corrected 3D reconstructions were calculated as described (Gabashvili et al., 2000). The final resolution was estimated by the Fourier Shell Correlation with a cutoff value of 0.5 (Table S1).

SPIDER was used for the computational separation of the cryo-EM reconstructions into densities corresponding to individual ribosomal subunits or IRES. The final maps were displayed with IRIS Explorer (Numerical Algorithms Group Inc., Downers Grove, IL) and Ribbons (Carson, 1991). Docking was done manually using O (Jones et al., 1991) and guided by a crosscorrelation-based 3D orientation search of certain parts of the cryo-EM maps in order to achieve optimal fit (Spahn et al., 2001b).

Acknowledgments

Supported in part by HHMI and NIH R037 GM29169, R01 GM55440, and P41 RR01219 (to J.F.); NSF DBI-9987844 (to A.M.); NIH (GM55979) (to P.S); DRG-1630 of the Damon Runyon Cancer Research Foundation (to E.J.); and the VolkswagenStiftung (to C.M.T.S.).

Received: March 23, 2004
Revised: June 22, 2004
Accepted: June 23, 2004
Published: August 19, 2004

References

Agrawal, R.K., Heagle, A.B., Penczek, P., Grassucci, R.A., and Frank, J. (1999). EF-G-dependent GTP hydrolysis induces translocation accompanied by large conformational changes in the 70S ribosome. Nat. Struct. Biol. *6*, 643–647.

Agrawal, R.K., Spahn, C.M.T., Penczek, P., Grassucci, R.A., Nierhaus, K.H., and Frank, J. (2000). Visualization of tRNA movements on the *Escherichia coli* 70S ribosome during the elongation cycle. J. Cell Biol. *150*, 447–459.

Alkemar, G., and Nygard, O. (2004). Secondary structure of two regions in expansion segments ES3 and ES6 with the potential of forming a tertiary interaction in eukaryotic 40S ribosomal subunits. RNA *10*, 403–411.

Beckmann, R., Spahn, C.M.T., Eswar, N., Helmers, J., Penczek, P.A., Sali, A., Frank, J., and Blobel, G. (2001). Architecture of the protein-conducting channel associated with the translating 80S ribosome. Cell *107*, 361–372.

Carson, M. (1991). Ribbons 2.0. J. Appl. Crystallogr. *24*, 103–106.

Carter, A.P., Clemons, W.M., Jr., Brodersen, D.E., Morgan-Warren, R.J., Hartsch, T., Wimberly, B.T., and Ramakrishnan, V. (2001). Crystal structure of an initiation factor bound to the 30S ribosomal subunit. Science *291*, 498–501.

Dever, T.E. (2002). Gene-specific regulation by general translation factors. Cell *108*, 545–556.

Doudna, J.A., and Rath, V.L. (2002). Structure and function of the eukaryotic ribosome: the next frontier. Cell *109*, 153–156.

Dube, P., Bacher, G., Stark, H., Müller, F., Zemlin, F., van Heel, M., and Brimacombe, R. (1998). Correlation of the expansion segments in mammalian rRNA with the fine structure of the 80 S ribosome; a cryoelectron microscopic reconstruction of the rabbit reticulocyte ribosome at 21 Å resolution. J. Mol. Biol. *279*, 403–421.

Dubochet, J., Adrian, M., Chang, J.J., Homo, J.C., Lepault, J., McDowall, A.W., and Schultz, P. (1988). Cryo-electron microscopy of vitrified specimens. Q. Rev. Biophys. *21*, 129–228.

Frank, J., and Agrawal, R.K. (2000). A ratchet-like inter-subunit reorganization of the ribosome during translocation. Nature *406*, 318–322.

Frank, J., Zhu, J., Penczek, P., Li, Y., Srivastava, S., Verschoor, A., Radermacher, M., Grassucci, R., Lata, R.K., and Agrawal, R.K. (1995). A model of protein synthesis based on cryo-electron microscopy of the *E. coli* ribosome. Nature *376*, 441–444.

Frank, J., Radermacher, M., Penczek, P., Zhu, J., Li, Y., Ladjadj, M., and Leith, A. (1996). SPIDER and WEB: processing and visualization of images in 3D electron microscopy and related fields. J. Struct. Biol. *116*, 190–199.

Frank, J., Penczek, P., Grassucci, R.A., Heagle, A., Spahn, C.M.T., and Agrawal, R.K. (2000). Cryo-electron microscopy of the translational apparatus: experimental evidence for the paths of mRNA, tRNA, and the polypeptide chain. In The Ribosome: Structure, Function, Antibiotics, and Cellular Interactions, R.A. Garrett, S.R. Douthwaite, A. Liljas, A.T. Matheson, P.B. Moore, and H.F. Noller, eds. (Washington, D.C.: ASM Press), pp. 45–51.

Gabashvili, I.S., Agrawal, R.K., Spahn, C.M.T., Grassucci, R.A., Frank, J., and Penczek, P. (2000). Solution structure of the *E. coli* 70S ribosome at 11.5 Å resolution. Cell *100*, 537–549.

Gao, H., Sengupta, J., Valle, M., Korostelev, A., Eswar, N., Stagg, S.M., Van Roey, P., Agrawal, R.K., Harvey, S.C., Sali, A., et al. (2003). Study of the structural dynamics of the *E coli* 70S ribosome using real-space refinement. Cell *113*, 789–801.

Gerbi, S.A. (1996). Expansion segment: regions of variable size that interrupt the universal core secondary structure of ribosomal RNA. In Ribosomal RNA: Structure, Evolution, Processing, and Function in Protein Synthesis, R.A. Zimmermann, and A.E. Dahlberg, eds. (New York: CRC Press), pp. 71–87.

Gomez-Lorenzo, M.G., Spahn, C.M.T., Agrawal, R.K., Grassucci, R.A., Penczek, P., Chakraburtty, K., Ballesta, J.P.G., Lavandera, J.L., Garcia-Bustos, J.F., and Frank, J. (2000). Three-dimensional cryo-electron microscopy localization of EF2 in the *Saccharomyces cerevisiae* 80S ribosome at 17.5 Å resolution. EMBO J. *19*, 2710–2718.

Hellen, C.U., and Sarnow, P. (2001). Internal ribosome entry sites in eukaryotic mRNA molecules. Genes Dev. *15*, 1593–1612.

Jan, E., and Sarnow, P. (2002). Factorless ribosome assembly on the internal ribosome entry site of cricket paralysis virus. J. Mol. Biol. *324*, 889–902.

Jan, E., Kinzy, G.T., and Sarnow, P. (2003). Divergent tRNA-like element supports initiation, elongation and termination of protein biosynthesis. Proc. Natl. Acad. Sci. USA *100*, 15410–15415.

Jones, T.A., Zou, J.Y., Cowan, S.W., and Kjeldgaard, M. (1991). Improved methods for building protein models in electron density maps and the location of errors in these models. Acta Crystallogr. A *A47*, 110–119.

Kanamori, Y., and Nakashima, N. (2001). A tertiary structure model of the internal ribosome entry site (IRES) for methionine-independent initiation of translation. RNA *7*, 266–274.

Lata, K.R., Agrawal, R.K., Penczek, P., Grassucci, R., Zhu, J., and Frank, J. (1996). Three-dimensional reconstruction of the *Escherichia coli* 30 S ribosomal subunit in ice. J. Mol. Biol. *262*, 43–52.

Matasova, N.B., Myltseva, S.V., Zenkova, M.A., Graifer, D.M., Vladimirov, S.N., and Karpova, G.G. (1991). Isolation of ribosomal subunits containing intact rRNA from human placenta: estimation of functional activity of 80S ribosomes. Anal. Biochem. *198*, 219–223.

Morgan, D.G., Ménétret, J.F., Radermacher, M., Neuhof, A., Akey, I.V., Rapoport, T.A., and Akey, C.W. (2000). A comparison of the yeast and rabbit 80S ribosome reveals the topology of the nascent chain exit tunnel, inter-subunit bridges and mammalian rRNA expansion segments. J. Mol. Biol. *301*, 301–321.

Morgan, D.G., Menetret, J.F., Neuhof, A., Rapoport, T.A., and Akey, C.W. (2002). Structure of the mammalian ribosome-channel complex at 17Å resolution. J. Mol. Biol. *324*, 871–886.

Nishiyama, T., Yamamoto, H., Shibuya, N., Hatakeyama, Y., Hachimori, A., Uchiumi, T., and Nakashima, N. (2003). Structural elements in the internal ribosome entry site of Plautia stali intestine virus responsible for binding with ribosomes. Nucleic Acids Res. *31*, 2434–2442.

Ogle, J.M., Murphy, F.V., Tarry, M.J., and Ramakrishnan, V. (2002). Selection of tRNA by the ribosome requires a transition from an open to a closed form. Cell *111*, 721–732.

Pestova, T.V., and Hellen, C.U. (2003). Translation elongation after assembly of ribosomes on the Cricket paralysis virus internal ribosomal entry site without initiation factors or initiator tRNA. Genes Dev. *17*, 181–186.

Pestova, T.V., Hellen, C.U., and Shatsky, I.N. (1996). Canonical eukaryotic initiation factors determine initiation of translation by internal ribosomal entry. Mol. Cell. Biol. *16*, 6859–6869.

Pestova, T.V., Shatsky, I.N., Fletcher, S.P., Jackson, R.J., and Hellen, C.U. (1998). A prokaryotic-like mode of cytoplasmic eukaryotic ribosome binding to the initiation codon during internal translation initiation of hepatitis C and classical swine fever virus RNAs. Genes Dev. *12*, 67–83.

Sachs, A.B. (2000). Cell cycle-dependent translation initiation: IRES elements prevail. Cell *101*, 243–245.

Sasaki, J., and Nakashima, N. (1999). Translation initiation at the CUU codon is mediated by the internal ribosome entry site of an insect picorna-like virus in vitro. J. Virol. *73*, 1219–1226.

Sasaki, J., and Nakashima, N. (2000). Methionine-independent initiation of translation in the capsid protein of an insect RNA virus. Proc. Natl. Acad. Sci. USA *97*, 1512–1515.

Schlünzen, F., Tocilj, A., Zarivach, R., Harms, J., Glühmann, M., Janell, D., Bashan, A., Bartels, H., Agmon, I., Franceschi, F., and Yonath, A. (2000). Structure of functionally activated small ribosomal subunit at 3.3 Å resolution. Cell *102*, 615–623.

Sonenberg, N., and Dever, T.E. (2003). Eukaryotic translation initiation factors and regulators. Curr. Opin. Struct. Biol. *13*, 56–63.

Spahn, C.M.T., Beckmann, R., Eswar, N., Penczek, P.A., Sali, A., Blobel, G., and Frank, J. (2001a). Structure of the 80S ribosome from *Saccharomyces cerevisiae*—tRNA-ribosome and subunit-subunit interactions. Cell *107*, 373–386.

Spahn, C.M.T., Blaha, G., Agrawal, R.K., Penczek, P., Grassucci, R.A., Trieber, C.A., Connell, S.R., Taylor, D.E., Nierhaus, K.H., and Frank, J. (2001b). Localization of the ribosomal protection protein Tet(O) on the ribosome and the mechanism of tetracycline resistance. Mol. Cell *7*, 1037–1045.

Spahn, C.M.T., Kieft, J.S., Grassucci, R.A., Penczek, P., Zhou, K., Doudna, J.A., and Frank, J. (2001c). Hepatitis C virus IRES RNA-induced changes in the conformation of the 40S ribosomal subunit. Science *291*, 1959–1962.

Spahn, C.M., Gomez-Lorenzo, M.G., Grassucci, R.A., Jorgensen, R., Andersen, G.R., Beckmann, R., Penczek, P.A., Ballesta, J.P., and Frank, J. (2004). Domain movements of elongation factor eEF2 and the eukaryotic 80S ribosome facilitate tRNA translocation. EMBO J. *23*, 1008–1019.

Stark, H., Rodnina, M.V., Wieden, H.J., van Heel, M., and Wintermeyer, W. (2000). Large-scale movement of elongation factor G and extensive conformational change of the ribosome during translocation. Cell *100*, 301–309.

Thompson, S.R., Gulyas, K.D., and Sarnow, P. (2001). Internal initiation in *Saccharomyces cerevisiae* mediated by an initiator tRNA/eIF2-independent internal ribosome entry site element. Proc. Natl. Acad. Sci. USA *98*, 12972–12977.

Vagner, S., Galy, B., and Pyronnet, S. (2001). Irresistible IRES: Attracting the translation machinery to internal ribosome entry sites. EMBO Rep. *2*, 893–898.

Valle, M., Zavialov, A., Sengupta, J., Rawat, U., Ehrenberg, M., and Frank, J. (2003). Locking and unlocking of ribosomal motions. Cell *114*, 123–134.

Wagenknecht, T., Grassucci, R., and Frank, J. (1988). Electron microscopy and computer image averaging of ice-embedded large ribosomal subunits from *Escherichia coli*. J. Mol. Biol. *199*, 137–147.

Wilson, J.E., Pestova, T.V., Hellen, C.U., and Sarnow, P. (2000a). Initiation of protein synthesis from the A site of the ribosome. Cell *102*, 511–520.

Wilson, J.E., Powell, M.J., Hoover, S.E., and Sarnow, P. (2000b). Naturally occurring dicistronic cricket paralysis virus RNA is regulated by two internal ribosome entry sites. Mol. Cell. Biol. *20*, 4990–4999.

Wimberly, B.T., Brodersen, D.E., Clemons, W.M., Jr., Morgan-Warren, R.J., Carter, A.P., Vonrhein, C., Hartsch, T., and Ramakrishnan, V. (2000). Structure of the 30S ribosomal subunit. Nature *407*, 327–339.

Yusupov, M.M., Yusupova, G.Z., Baucom, A., Lieberman, K., Earnest, T.N., Cate, J.H., and Noller, H.F. (2001). Crystal structure of the ribosome at 5.5 Å resolution. Science *292*, 883–896.

Yusupova, G.Z., Yusupov, M.M., Cate, J.H., and Noller, H.F. (2001). The path of messenger RNA through the ribosome. Cell *106*, 233–241.

Accession Numbers

The cryo-EM density maps of human 40S-CrPV-IRES, 80S-CrPV-IRES, 40S (vacant) and 80S (vacant) ribosomes have been deposited at the Macromolecular Structure Database of the EMBL-European Bioinformatics Institute, Cambridge, UK, with accession numbers EMD-1090, EMD-1091, EMD1092, and EMD1093, respectively.